Preliminary development of anatomically realistic breast tumor models for microwave imaging

Ana Catarina Pelicano[1], Nuno A. M. Araújo[2], Raquel C. Conceição[1]
[1] Instituto de Biofísica e Engenharia Biomédica, Faculdade de Ciências da Universidade de Lisboa, Campo Grande, 1749-016 Lisbon, Portugal, acpelicano@fc.ul.pt, rcconceicao@fc.ul.pt
[2] Centro de Física Teórica e Computacional, Faculdade de Ciências da Universidade de Lisboa, Campo Grande, 1749-016 Lisbon, Portugal, nmaraujo@fc.ul.pt

***Abstract* — In this work, we present a preliminary study of three classifiers – Linear Discriminant Analysis (LDA), Support Vector Machines (SVMs) and *k*-Nearest Neighbors (*k*NN) – to differentiate between malignant and benign tumors extracted from Magnetic Resonance (MR) images, based on their morphological features. The dataset in this study comprises 24 tumors: 12 malignant and 12 benign. Twelve morphological features were initially considered for tumor classification. The Mann-Whitney test was employed for feature selection, and the performance of the classifiers was evaluated with accuracy, sensitivity, specificity, F1-score and Matthew's Correlation Coefficient (MCC) metrics. *k*NN (with *k*=6 and Chebyshev distance) outperformed the other classifiers with an accuracy, sensitivity, and specificity of 87.5%, 83.3% and 91.7%, respectively.**

***Index Terms* — breast cancer, tumor classification, morphological features.**

I. Introduction

In 2020, breast cancer reported over 2.2 million new cases, reaching the top of the most common types of cancers worldwide. It was also the fifth deadliest type of cancer with over 684.000 deaths in 2020 [1]. Early-stage diagnosis is the key for a successful treatment outcome, thereby improving the quality of life of cancer patients and survival rates.

MicroWave Imaging (MWI) systems have been studied for early-stage breast cancer diagnosis [2-4] due to differences in dielectric properties between benign and malignant tissues at microwave frequencies [5]. To ensure the robustness and good performance of MWI systems in detecting and classifying breast tumors, complex scenarios mimicking the realistic conditions of a clinical exam must be tested. Hence, realistic models of breast tumors are needed.

Malignant breast tumors generally have an irregular shape surrounded with spicules whereas benign tumors present roughly rounded or elliptical shapes [6,7]. So far, most of the breast models reported in literature to test MWI systems present an unrealistic simplified shape, generally, spherical, elliptical, and cylindrical. Mimicking tissues and structures inside the breast also tend to be represented by simplified shapes. In [8], spherical glass bulbs with 5, 10 and 15mm radii containing saline solutions were used to mimic tumor tissues in phantom studies. An ellipsoid container with internal dimensions 10- and 20mm was 3D printed in [9] to study the feasibility of a radar-based breast MWI dry setup. A 20mm spherical phantom filled with a 10:90 ratio of water to glycerin was used to emulate a breast tumor in [10]. Two cylindrical shaped tumor phantoms with 10 and 20mm diameters and 30mm height were tested in [11]. A small cylindrical plastic container filled with water was used as a breast tumor phantom in experimental tests in [12].

More realistic breast tumors have been modelled with Gaussian Random Spheres and used for validation tests of a microwave imaging device in [13], and for tumor classification using a MWI prototype system in [14]. In [15], realistic benign and malignant breast phantoms were carved by hand resulting in approximately spherical and spiculated models for benign and malignant tumors, respectively. To emphasize that none are based on accurate anatomical representations of tumors.

We aim to address a gap in literature: the lack of realistic breast tumor phantoms for MWI prototype testing. Hence, we have been preparing accurate MRI-derived models of the breast, which will be later 3D printed. In this paper, we evaluate the discriminative power of tumor morphological features in breast tumor classification.

II. Materials and Methods

A. Dataset

The dataset in this study comprises 24 breast tumors: 12 malignant (scored with BI-RADS 5/6) and 12 benign (BI-RADS 2/3) [6], which were segmented from breast MR images collected at Hospital da Luz – Lisboa. The clinical protocol included the acquisition of a Dynamic Contrast Enhanced (DCE) three-dimensional (3D) T1-weighted Fast Low Angle Shot 3D (fl3D) Spectral Attenuated Inversion Recovery (SPAIR) sequence, consisting of 6 sets of images: an image before the injection of gadolinium and 5 post-contrast images. Subtractions of each post-contrast image from the pre-contrast image are also provided to enhance tumor regions and annul hypersignal regions formerly present in the pre-contrast image. For each case, the breast tumor was segmented from the subtraction image which provided better segmentation between tumor and non-

tumorous tissues. One must note that a larger tumor will require more time of contrast uptake to be revealed.

This study was approved by the Scientific and Ethical Commission of Hospital da Luz – Lisboa, under references CES/44/2019/ME and CES/34/2020/ME.

B. Tumor Segmentation

A pre-processing segmentation pipeline was applied to the breast MR scans before tumor segmentation. The developed pipeline included: (i) correction of the bias field – an artifact which corrupts the grey level values across the image [16], (ii) data normalization between 0 and 255 using the Minimum-Maximum normalization approach [17], (iii) background subtraction using the Otsu's method to create a binary mask of the body, followed by the implementation of (iv) a 3-by-3-by-3 median filter for edge smoothing [18]. Note: step (iv) of the pre-processing pipeline is removed in the case of infra-centimetric tumors as it produces substantial changes in the size and shape of tumors.

A 3D region growing algorithm, based on [19], was implemented for tumor segmentation. The algorithm allows the growth of a region to adjacent points p_{adj}, whose intensity satisfy the condition:

$$seed\ value - threshold \leq p_{adj} \leq seed\ value + threshold \quad (1)$$

The seed of the algorithm – point from where the region starts growing – was automatically set to the highest intensity pixel of the slice provided by the user, and the lower bound of threshold was defined by the mean minus three times the standard-deviation of all body voxels. Both parameters should be confirmed and manually corrected, if necessary, especially in the case of large heterogeneous malignant tumors comprising a wide range of intensity values. The Hoshen-Kopelman algorithm [20] was used isolate the tumor region, by iteratively identifying the neighboring pixels to be included in the growing region. The developed segmentation procedure is detailed in [21].

C. Morphological Features

Twelve morphological features were extracted from the segmented breast tumors: (i) number of voxels of the tumor, No. Voxels, (ii) length of the larger axis in each dimension, Length, (iii) radius of gyration [22], (iv) inertia tensor [23], (v) volume, (vi) surface area, (vii) compactness, (viii) sphericity, (ix) Normalized Radial Length (NRL) mean, (x) NRL entropy, (xi) NRL ratio, and (xii) roughness [24]. Compactness and sphericity provide a general knowledge of the tumor shape, high levels of compactness and sphericity are expected for round-shaped structures whereas irregular-shaped structures, such as malignant tumors, are expected to present lower indexes of compactness and sphericity. The NRL-based features provide finer detail of shape, where NRL is the normalized Euclidean distance from center of mass to the contour pixels of the object.

D. Feature Selection

The nonparametric Mann–Whitney test was used for feature selection. Two independent populations were established: malignant versus benign tumors. The Mann-Whitney compares the median values of each feature in the malignant and benign groups [25]. Hence, features whose median values showed a statistically significant difference between the two groups were selected for the classification algorithms. A *p-value* < 0.01 was considered significant for all tests.

E. Classification Algorithms

Three classifiers – LDA, SVMs and *k*NN – were studied to obtain an optimal classifier to differentiate between benign and malignant tumors based on morphologic features. The diagnostic performance of the classifiers was evaluated with accuracy, sensitivity, specificity, F1-score [26] and Matthew's Correlation Coefficient (MCC) metrics [27].

As a pre-processing step, the selected morphologic features values were normalized to have zero mean and unit variance, since their values present different orders of magnitude. Then, the three classifiers were implemented.

LDA classifier uses a linear function to discriminate classes with the same covariance matrix and multivariate normal Gaussian distributions [28]. *k*NN is a supervised machine learning algorithm which classifies a new observation based on the most common class among its *k*-nearest neighbors. The *k*-nearest neighbors are determined based on a similarity measure, i.e., distance [26]. Both parameters, *k* and distance, must be optimized. We tested k = 1, 2, …, 11 and considered four distances: Manhattan, Hamming, Chebyshev and Euclidean. The SVM methods allow the classification of either linear or nonlinear separable datasets. The original training data are transformed to a higher dimension by means of a kernel. We used the Radial Basis Function (RBF) kernel. Within the new dimension, the SVM algorithm searches for the optimal linear hyperplane which separates the training data into two classes [26].

Leave-One-Out cross validation was implemented to ensure robustness and prevent overfitting.

III. Results and Discussion

A. Tumor segmentation

Fig. 1 and 2 depict the results of the developed segmentation procedure of an extremely heterogeneous malignant tumor. Fig 1 shows the effects of the correction of the bias field, applied in a). The inhomogeneity between voxels intensities, shown in b) is corrected in c). Fig 2 shows the results for each step of the developed tumor segmentation pipeline. In a) we present the torso mask used for background subtraction, the application of the median filter for edge smoothing is depicted in b), c) shows the segmented tumor, in white, resulting from the 3D region growing algorithm and d) the final tumor after the application of the Hoshen-Kopelman algorithm.

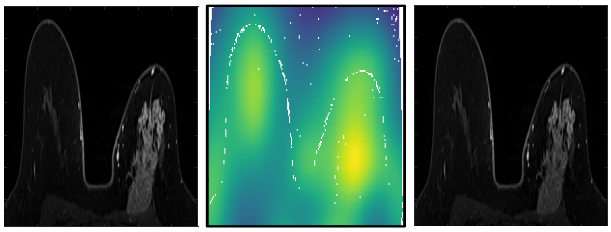

a) b) c)

Fig. 1. Correction of the bias field. a) image of the original exam, b) image with the inhomogeneity between the voxels intensities and c) corrected image.

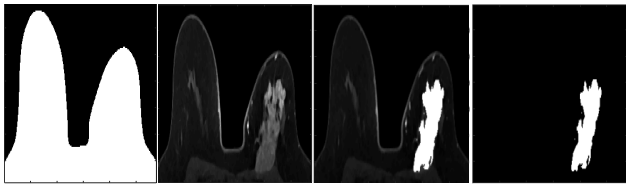

a) b) c) d)

Fig. 2. Results of each step of the developed tumor segmentation pipeline. a) torso mask for background subtraction, b) median filtering for edge smoothing, c) segmented tumor, in white, resulting from the 3D region growing algorithm and d) final tumor after the application of the Hoshen-Kopelman algorithm.

TABLE I. MEDIAN, STANDARD DEVIATION AND P-VALUE OF EACH MORPHOLOGICAL FEATURE.

Morphological Features	**Benign Tumors**	**Malignant tumors**	***p-value***
	Median	***Median***	
No. Voxels	102.5	970	**0.001**
Length	6.5	14.5	**0.001**
Radius of Gyration	1.574	3.837	**0.002**
Inertia Tensor	429.5	2.855e+4	**0.001**
Volume	111.2	963.3	**0.001**
Surface Area	64.06	470.9	**0.001**
Compactness	47.40	243.6	**0.002**
Sphericity	3.258	2.556	0.236
NRL mean	0.588	0.383	0.035
NRL entropy	5.898	8.785	**0.001**
NRL ratio	0.128	0.146	0.436
Roughness	0.078	0.200	0.030

B. *Feature Selection*

Table I reports the median value of each morphological feature in both groups, and the *p-value* calculated from the Mann-Whitney test.

TABLE II. OPTIMAL DIAGNOSTIC PERFORMANCE OF THE LDA, SVMS AND KNN CLASSIFIERS.

	Accuracy	**Sensitivity**	**Specificity**	**F1-score**	**MCC**
LDA	0.583	0.417	0.750	0.500	0.177
SVMs	0.833	0.750	0.917	0.818	0.676
***k*NN**	**0.875**	**0.833**	**0.917**	**0.869**	**0.753**

The median values of all morphological features presented a statistically significant difference between the benign and malignant groups, except sphericity, NRL mean, NRL ratio and roughness. The remaining features were included in the study of three classifiers – LDA, SVMs and *k*NN – to differentiate between malignant and benign tumors.

C. *Classification Algorithms*

Table II reports the optimal diagnostic performance of the LDA, SVMs and *k*NN classifiers. Chebyshev distance and a number of *k*-nearest neighbors of 6 were the optimal parameters obtained for the *k*NN classifier. The *k*NN classifier outperformed LDA and SVMs classifiers.

IV. CONCLUSIONS AND FUTURE WORK

The developed segmentation framework is suitable to segment tumors with a varying level of heterogeneity regarding voxel intensity. The proposed pipeline is flexible since it does not operate under the assumption that generally, biological tissues are well separated within the grayscale of the image. The realistic breast tumors derived from MRI exams will be 3D printed and used to test a MWI prototype system for real-time breast tumor diagnosis. The use of accurate anatomically realistic tumor models will be a novelty in the experimental MWI testing field.

From the initially considered twelve morphological features, only eight – No. Voxels, length, radius of gyration, inertia tensor, volume, surface area, compactness and NRL entropy – were found statistically significant for a significance level of 0.01.

The *k*NN classifier (with k=6 and Chebyshev distance) outperformed LDA and SVMs classifiers. Additionally, the results of this study indicate the importance of shape information in predicting breast tumor type (benign or malignant), which will be included in MWI future studies.

Moreover, future classification work will also include texture features to study and optimize the performance of the classifiers.

ACKNOWLEDGMENT

This research was funded by Fundação para a Ciência e Tecnologia (FCT) under the fellowship UI/BD/150762/2020, FCT/MET (PIDDAC) under the Strategic Program UIDB/00645/2020 and under Contracts no. PTDC/FIS-MAC/28146/2017 (LISBOA-01-0145-FEDER-028146),

UIDB/00618/2020, and UIDP/00618/2020. The authors would like to acknowledge the study with references CES/44/2019/ME (19/09/2019) and CES/34/2020/ME (06/11/2020) in Hospital da Luz – Lisboa and their staff (Dr. M. Lurdes Orvalho and Tiago Castela) for the MRI acquisitions. This work is developed in the framework of COST Action CA17115 – MyWAVE.

REFERENCES

[1] International Agency for Research on Cancer, "World Health Organization, GLOBOCAN 2020: Estimated Cancer Incidence, Mortality and Prevalence Worldwide in 2020 – Cancer Fact Sheets", Acessed: https://gco.iarc.fr/today/data/factsheets/cancers/.

[2] E. Fear, S. Hagness, M. Stuchly, "Confocal microwave imaging for breast cancer detection: localization of tumors in three dimensions," IEEE TBME, vol. 49(8), pp.812-822, 2002.

[3] D. Flores-Tapia, S. Pistorius, "Real time breast microwave radar image reconstruction using circular holography: a study of experimental feasibility," Med. Phys., vol. 38(10), pp.5420-5431, 2011.

[4] A. Preece, I. Craddock, M. Shere, L. Jones, H. Winton, "MARIA M4: clinical evaluation of a prototype ultrawideband radar scanner for breast cancer detection," J. Med. Imaging, vol. 3(3), 2016.

[5] M. Lazebnik et al., "A large-scale study of the ultrawideband microwave dielectric properties of normal, benign and malignant breast tissues obtained from cancer surgeries," Phys. Med. Biol., vol. 52(20), pp. 6093-6115, 2007.

[6] C. D'Orsi, E. Sickles, E. Mendelson and E. Morris, ACR BI-RADS Atlas, breast imaging reporting and data system, American College of Radiology: Reston, VA,USA, 2013.

[7] R. Rangayyan, N. El-Faramawy, J. Desautels, O. Alim, "Measures of acutance and shape for classification of breast tumors," IEEE Trans. Med. Imaging, vol. 16, pp. 799-810, 1997.

[8] T. Reimer, J. Krenkevich, S. Pistorius, " An open-access experimental dataset for breast microwave imaging," 14th European Conference on Antennas and Propagation (EuCAP), pp. 1-5, 2011.

[9] J. Felício, J. Bioucas-Dias, J. Costa, C. Fernandes, "Microwave breast imaging using a dry setup," IEEE Trans. Comput. Imaging, vol. 6, pp.167-180, 2020.

[10] V. Khoshdel, M. Asefi, A. Ashraf, J. LoVetri, " Full 3D microwave breast imaging using a deep-learning technique," J. Imaging, vol. 6(8), 2020.

[11] E. Porter, J. Fakhoury, R. Oprisor, M. Coates and M. Popovic, "Improved tissue phantoms for experimental validation of microwave breast cancer detection," in Proceedings of the 4th European Conference on Antennas and Propagation, Barcelona, Spain, 2010.

[12] S. Salvador, G. Vecchi, "Experimental tests of microwave breast cancer detection on phantoms," IEEE Trans. Antennas Propag., vol. 57(6), pp. 1705-1712, 2009.

[13] A. Fasoula et al., "On-site validation of a microwave breast imaging system, befre first patient study," Diagnostics, vol. 8, 2018.

[14] R. Conceição, "Classification of breast tumour models with a prototype microwave imaging system," Medical Physics, vol. 47(4), pp. 1860-1870, 2020.

[15] B. Oliveira et al., "Microwave breast imaging: experimental tumour phantoms for the evaluation of new breast cancer diagnosis system," Biomed. Phys. Eng. Express, vol. 4, 2018.

[16] U. Vovk, F. Pernus, B. Lika, "A review of methods for correction of intensity inhomogeneity in MRI," IEEE Trans. Med. Imaging, vol. 26, pp. 405-421, 2007.

[17] S. Patro, K. Sahu, "Normalization: a preprocessing stage," CoRR, vol. abs/1503.06462, 2015.

[18] R. Gonzalez, R. Woods, Digital image processing, New Jersey: Prentice Hall, 2002.

[19] D. Kroon. (2021) Region Growing, MATLAB Central File Exchange. Accessed:https://www.mathworks.com/matlabcentral/fileexchange/19084-region-growing.

[20] J. Hoshen, R. Kopelman, "Percolation and cluster distribution. I. Cluster multiple labeling technique and critical concentration algorithhm," Phys. Rev. B, vol. 14(8), pp. 3438-3445, 1976.

[21] A. Pelicano *et al.,"*Development of 3D MRI-Based Anatomically Realistic Models of Breast Tissues and Tumours for Microwave Imaging Diagnosis", Sensors, vol. 21(24):8265, 2021.

[22] D. Drasco, S. Hoehme, "Modeling the impact of granular embedding media, and pulling versus pushing cells on growing cell clones," New J. Phys., vol. 14, 2012.

[23] J. Peraire, J. Widnall, "Lecture L26 - 3D Rigid Body Dynamics : The Inertia Tensor," Dynamics, 2008.

[24] K. Nie et al.,"Quantitative analysis of lesion morphology and texture features for diagnostic prediction in breast MRI," Acad. Radiol., vol.15(12), pp.1513-1525, 2008.

[25] J. Gibbons, S. Chakraborti. Nonparametric Statistical Inference, 5th ed., Boca Raton, FL: Chapman & Hall/CRC Press, 2011.

[26] J. Han, M. Kramer, J. Pei, Data Mining: Concepts and Techniques, 3rd ed., MA, USA: Elsevier, 2012.

[27] D. Chicco, G. Jurman, "The advantages of the Matthews correlation coefficient (MCC) over F1 score and accuracy in binary classification evaluation," BMC Genom., vol. 21, 2020.

[28] J. Hair, W. Black, B. Babin, R. Anderson, Multivariate Data Analysis, 7th ed., Upper Saddle River: Prentice Hall, 2009.